Supporting Information

Replacement of the Distal Histidine Reveals a Non-Canonical Heme Binding Site in a 2-on-2 Hemoglobin

Dillon B. Nye and Juliette T. J. Lecomte*

T. C. Jenkins Department of Biophysics, Johns Hopkins University, Baltimore, MD, 21218, United States

Table S1. ^{1}H assignments and selected ^{1}H T_1 values for the mesoheme in H46L and H46L/Q47L mesoGlbN*[a]

	H46L		H46L/Q47L	
A	δ (ppm)	T_1 (ms)	δ (ppm)	T_1 (ms)
1-CH_3	12.71	85	11.43	85
3-CH_3	15.48	120	16.14	115
5-CH_3	13.71	85	12.96	85
8-CH_3	1.28		1.92	
2-CαH1	12.48	90	11.12	80
2-CαH2	13.12		13.66	
2-CβH_3	–0.06		–0.28	
4-CαH1	–3.26		–3.01	110
4-CαH2	–0.34		–0.03	
4-CβH_3	–0.34		–0.27	
6-CαH1	14.99	100	14.60	100
6-CαH2	10.10		9.94	90
6-CβH1	–1.30	90	–1.44	100
6-CβH2	–0.89		–0.99	
7 CαH1	3.86		4.18	
7-CαH2	7.53		7.93	
7-CβH1	–1.96	110	–2.01	110
7-CβH2	–2.76	90	–2.78	
α-meso	–2.57	30	–2.81	
β-meso	8.05		8.06	
γ-meso	–3.28		–3.50	
δ-meso	8.83		8.86	30

[a]Data at 25 °C, 99% $^{2}H_2O$, pH* 7.2 or 7.3. Standard errors in the T_1 values determined by curve fitting do not exceed 5% (see Figure S1).

Table S2. ^{1}H, ^{15}N and ^{13}C chemical shifts for selected residues in H46L/Q47L mesoGlbN*[a]

#	ID	N	C	C^{α}	C^{β}	C^{γ}	$C^{\delta1}$	$C^{\delta2}$	H^{N}	H^{α}	$H^{\beta2}$	$H^{\beta3}$	H^{γ}	$H^{\delta1}$	$H^{\delta2}$		
4	Leu	124.4	177.1	58.5	40.7	N.D.	22.9	26.5	9.21	3.90	1.66	1.90	1.01	0.81	0.52		
8	Leu	116.0	175.8	56.1	43.3	N.D.	24.2	26.7	8.08	3.82	1.16	1.62	1.58	0.58	0.28		
46	Leu	120.8	179.5	57.8	42.6	27.5	24.8	24.8	8.52	4.52	2.08	2.13	2.04	1.31	1.29		
47	Leu	122.1	179.2	58.0	39.0	N.D	23.4	26.5	9.46	4.52	2.17	2.36	1.62	0.89	0.71		
73	Leu	117.9	178.2	56.7	46.8	N.D.	26.4	24.9	9.03	5.37	1.99	3.66	2.51	1.15	1.43		
79	Leu	118.2	175.8	54.5	42.5	N.D.	24.0	25.5	5.83	3.30	–0.02	0.45	0.32	–0.56	0.04		
91	Leu	124.7	177.6	58.8	40.8	26.9	20.7	24.9	7.93	3.93	0.71	1.71	1.17	0.08	0.41		
95	Leu	119.3	178.6	57.6	41.0	N.D.	27.5	22.1	7.33	4.1	1.15	1.97	N.D.	0.91	0.79		
104	Leu	120.9	179.2	56.6	41.1	N.D.	26.1	23.6	7.30	4.23	1.15	1.77	1.62	0.78	0.69		
122	Leu	124.0	176.9	55.4	42.4	27.3	24.8	23.5	8.28	4.36	1.59	1.70	1.75	0.83	0.99		
		N	C	C^{α}	C^{β}	C^{γ}	$C^{\delta1/\delta2}$	$C^{\varepsilon1/\varepsilon2}$	C^{ζ}	H^{N}	H^{α}	$H^{\beta2}$	$H^{\beta3}$	$H^{\delta1/\delta2}$	$H^{\varepsilon1/\varepsilon2}$	H^{ζ}	
21	Phe	124.4	176.9	59.8	38.5	N.D.	131.0	130.6	127.6	8.91	4.23	2.87	2.97	5.98	6.30	5.77	
34	Phe	119.3	175.2	60.5	37.3	N.D.	133.3	N.D.	N.D.	6.98	3.94	2.06	2.34	6.89	6.64	6.83	
35	Phe	114.0	175.4	57.7	39.4	N.D.	N.D.	N.D.	128.4	7.28	4.10	2.35	3.50	6.74	6.89	6.68	
50	Phe	120.5	177.8	61.8	41.2	N.D.	132.2	130.7	130.4	9.10	4.32	3.36	3.60	7.29	7.35	5.97	
55	Phe	112.0	175.3	52.7	36.9	N.D.	133.3	131.1	128.7	8.12	4.93	3.26	3.47	6.81	6.90	6.80	
84	Phe	117.3	174.5	62.8	38.9	N.D.	N.D.	N.D.	N.D.	6.54	1.49	1.45	2.54	4.86	8.40	10.45	
		N	C	C^{α}	C^{β}	C^{γ}	$C^{\delta1/\delta2}$	$C^{\varepsilon1/\varepsilon2}$	C^{ζ}	H^{N}	H^{α}	$H^{\beta2}$	$H^{\beta3}$	$H^{\delta1/\delta2}$	$H^{\varepsilon1/\varepsilon2}$	H^{ζ}	H^{η}
22	Tyr	116.5	177.9	63.4	37.1	N.D.	132.3	118.0	N.D.	7.97	3.51	2.54	2.61	6.53	6.51	-	9.98
		N	C	C^{α}	C^{β}	$C^{\gamma1}$	$C^{\gamma2}$	$C^{\delta1}$	H^{N}	H^{α}	H^{β}	$H^{\gamma11}$	$H^{\gamma12}$	$H^{\gamma2}$	$H^{\delta1}$		
31	Ile	103.4	177.0	60.8	42.9	24.3	18.2	14.8	6.89	4.57	1.82	0.62	N.D.	0.44	0.27		
		N	C	C^{α}	C^{β}	$C^{\gamma1}$	$C^{\gamma2}$	H^{N}	H^{α}	H^{β}	$H^{\gamma1}$	$H^{\gamma2}$					
18	Val	115.9	177.2	67.4	31.0	23.4	23.7	8.21	3.41	2.19	1.49	0.95					
25	Val	121.8	177.5	66.5	31.3	20.9	21.5	8.31	3.00	1.30	–0.19	–0.47					
74	Val	119.3	177.6	65.0	34.1	21.4	20.7	9.85	4.20	5.74	0.22	–1.21					
87	Val	113.9	176.7	65.2	30.2	21.3	21.4	6.49	2.69	0.04	–1.03	–0.51					
108	Val	120.6	179.0	66.7	30.8	23.2	21.0	8.33	3.52	2.41	0.70	0.96					
121	Val	119.1	176.3	62.7	32.6	20.6	20.6	8.12	4.19	2.25	0.97	1.04					
		N	C	C^{α}	C^{β}	C^{γ}	C^{ε}	H^{N}	H^{α}	$H^{\beta2}$	$H^{\beta3}$	$H^{\gamma2}$	$H^{\gamma3}$	H^{ε}			
40	Met	127.8	178.8	55.2	28.6	N.D.	14.6	8.73	4.29	N.D.	1.79	N.D.	2.66	1.29			
66	Met	116.4	178.7	57.4	30.9	N.D.	16.1	7.84	4.33	1.20	1.47	1.60	1.92	0.76			
		N	C	C^{α}	C^{β}	H^{N}	H^{α}	H^{β}									
69	Ala	123.8	181.4	55.8	18.9	9.22	4.91	1.93									
112	Ala	119.6	177.6	53.0	21.9	9.25	5.71	1.56									
114	Ala	131.0	N.D.	59.6	17.0	12.01	6.81	2.67									
116	Ala	118.6	180.1	55.0	21.1	8.68	5.15	3.04									
		N	C	C^{α}	C^{β}	C^{γ}	H^{N}	H^{α}	$H^{\beta2}$	$H^{\beta3}$	$H^{\gamma2}$	$H^{\gamma3}$					
43	Gln	116.5	176.9	58.6	27.3	35.1	7.52	4.05	1.72	2.23	N.D.	N.D.					
107	Glu	119.8	179.5	60.2	29.9	36.7	7.46	5.21	2.20	2.24	2.60	N.D.					

[a]Data at 25 °C, 5–10% $^{2}H_2O$, pH* 7.1–7.3. Several stereospecific assignments were made arbitrarily by comparison to the WT GlbN structure; N.D., not determined.

Table S3A. Selected protein–mesoheme NOEs observed in H46L/Q47L mesoGlbN*[a]

proton(s) 1	proton(s) 2[b]	WT GlbN-CN?[c]	WT GlbN?[d]	Figure
1-CH_3	L47 $H^{\delta1}$	+	−	S10A
1-CH_3	F50 $H^{\varepsilon1/\varepsilon2}$	+	−	S10B
1-CH_3	L51 $H^{\delta2}$	+	−	S10A
1-CH_3	L91 $H^{\delta2}$	+	−	S10A
1-CH_3	A112 H^{β}	+	−	S10A
2-CH_3	V87 $H^{\gamma1}$	+	+	
3-CH_3	V74 $H^{\gamma1}$	−	−	S10A
3-CH_3	L79 $H^{\delta1}$	+	+	S10A
3-CH_3	L79 $H^{\delta2}$	+	+	S10A
3-CH_3	F84 H^{α}	+	+	S10A
3-CH_3	F84 $H^{\beta1}$	+	+	
3-CH_3	F84 $H^{\delta1/\delta2}$	+	+	
3-CH_3	V87 H^{β}	+	+	S10A
3-CH_3	V87 $H^{\gamma1}$	+	+	S10A
3-CH_3	V87 $H^{\gamma2}$	+	+	S10A
4-CH_3	N80 H^{α}	−	−	
5-CH_3	V121 $H^{\gamma1}$	−	−	S10B
5-CH_3	V121 H^{β}	−	−	S10B
5-CH_3	L122 $H^{\delta1}$	−	−	S10B
5-CH_3	L122 $H^{\delta2}$	−	−	S10B
5-CH_3	L122 H^{α}	−	−	S10B
7-$C\beta H_2$	M66 H^{ε}	+	+	S10B
7-$C\beta H_2$	M66 $H^{\beta3}$	−	−	S10B
7-$C\beta H_2$	M66 $H^{\beta2}$	−	−	S10B
7-$C\beta H_2$	M66 H^{α}	+	+	S10B
8-CH_3	A112 H^{α}	−	−	S8B
8-CH_3	F50 H^{ζ}	+	−	S8B

[a]Data at 25 °C, 10% or 99% ^2H_2O, pH* 7.1–7.3. [b]Several stereospecific assignments were made arbitrarily by comparison to the WT GlbN structure. [c]Comparison of the observed NOEs with expectations based on the crystal structure of cyanomet WT GlbN (PDB ID: 1S69). An NOE is predicted by the structure if the protons are within 6 Å. [d]Same prediction, using *bis*-histidine WT GlbN (PDB ID: 1RTX). Both X-ray structures have the His117–heme PTM.

Table S3B. Selected intraprotein NOEs observed in H46L/Q47L mesoGlbN*[a]

proton(s) 1[b]	proton(s) 2[b]	WT GlbN-CN?[c]	WT GlbN?[d]	Figure
L4 $H^{\delta2}$	F55 H^{α}	+	+	S8A
L4 $H^{\delta2}$	F55 $H^{\delta1/\delta2}$	+	+	S8A
L4 $H^{\delta2}$	L104 H^{α}	+	−	S8A
L4 $H^{\delta2}$	E107 $H^{\beta2}$	+	−	S8A
L4 $H^{\delta2}$	V108 H^{α}	+	−	S8A
L8 $H^{\delta2}$	F55 $H^{\delta1/\delta2}$	+	+	S8B
L8 $H^{\delta2}$	F55 $H^{\varepsilon1/\varepsilon2}$	+	+	S8B
L8 $H^{\delta2}$	F55 H^{ζ}	+	+	S8B
V18 H^{α}	L47 $H^{\delta2}$	+	−	S9
F21 $H^{\varepsilon1/\varepsilon2}$	Y22 H^{η}	+	−	S9
F21 $H^{\delta1/\delta2}$	V25 $H^{\gamma1}$	+	+	S8A,B
F21 H^{ζ}	V87 $H^{\gamma2}$	+	+	S8A,B
F21 $H^{\delta1/\delta2}$	L47 $H^{\delta2}$	+	+	S9, S8B
F21 $H^{\varepsilon1/\varepsilon2}$	L47 $H^{\delta2}$	+	+	S9
F21 $H^{\delta1/\delta2}$	L91 $H^{\delta2}$	+	+	S8B
F21 $H^{\varepsilon1/\varepsilon2}$	L91 $H^{\delta2}$	+	+	S8B
Y22 $H^{\varepsilon1/\varepsilon2}$	V25 $H^{\gamma1}$	+	−	S8A,B
Y22 $H^{\varepsilon1/\varepsilon2}$	V25 $H^{\gamma2}$	+	−	S8B
Y22 $H^{\delta1/\delta2}$	M40 $H^{\varepsilon1}$	+	−	S8B
Y22 $H^{\varepsilon1/\varepsilon2}$	L47 $H^{\delta2}$	+	+	S9
Y22 H^{η}	L47 $H^{\delta2}$	+	−	S9
Y22 H^{η}	L73 $H^{\delta2}$	−	−	S9
Y22 $H^{\varepsilon1/\varepsilon2}$	L73 $H^{\delta2}$	−	−	
V25 $H^{\gamma1}$	V87 $H^{\gamma1}$	+	+	S8A
F34 $H^{\delta1/\delta2}$	L79 $H^{\delta2}$	+	+	S8B
F35 H^{ζ}	L79 $H^{\delta2}$	+	−	S8B
Q43 H^{α}	L73 $H^{\delta2}$	−	−	8
L47 H^{α}	L73 $H^{\delta1}$	−	−	8
L47 H^{α}	L73 $H^{\delta2}$	−	−	8
F50 $H^{\delta1/\delta2}$	A69 H^{β}	−	−	8
F50 $H^{\varepsilon1/\varepsilon2}$	H70 $H^{\beta3}$	−	−	S10B
F50 $H^{\varepsilon1/\varepsilon2}$	H70 $H^{\beta2}$	−	−	S10B
F50 $H^{\beta1}$	L73 $H^{\delta1}$	−	−	8
F50 $H^{\delta1/\delta2}$	L73 $H^{\delta1}$	−	−	8
L51 $H^{\delta21}$	F55 H^{ζ}	+	+	S8B
F55 $H^{\varepsilon1/\varepsilon2}$	V108 $H^{\gamma1}$	+	+	
M66 H^{α}	A69 H^{β}	+	+	8
H70 H^{α}	L73 $H^{\delta1}$	+	+	8
H77 $H^{\delta2}$	L79 $H^{\delta2}$	−	−	S8B
F84 H^{ζ}	G113 $H^{\alpha3}$	+	+	S10B
F84 H^{ζ}	A114 H^{α}	−	−	S10B
F84 $H^{\varepsilon1/\varepsilon2}$	A114 H^{α}	−	−	S10B
F84 H^{ζ}	H117 $H^{\beta3}$	+	+	S10B
L92 $H^{\delta1}$	A109 H^{α}	+	+	
L92 $H^{\delta1}$	G113 $H^{\alpha3}$	+	−	
A114 H^{α}	H117 $H^{\beta3}$	+	+	S10B

[a]Data at 25 °C, 10% or 99% ^2H_2O, pH* 7.1–7.3. [b]Several stereospecific assignments were made arbitrarily by comparison to the WT GlbN structure. [c]Comparison of the observed NOEs with the crystal structure of cyanomet WT GlbN (PDB ID: 1S69). An NOE is predicted by the structure if the protons are within 6 Å. [d]Same prediction, using *bis*-histidine WT GlbN (PDB ID: 1RTX). Both X-ray structures have the His117–heme PTM.

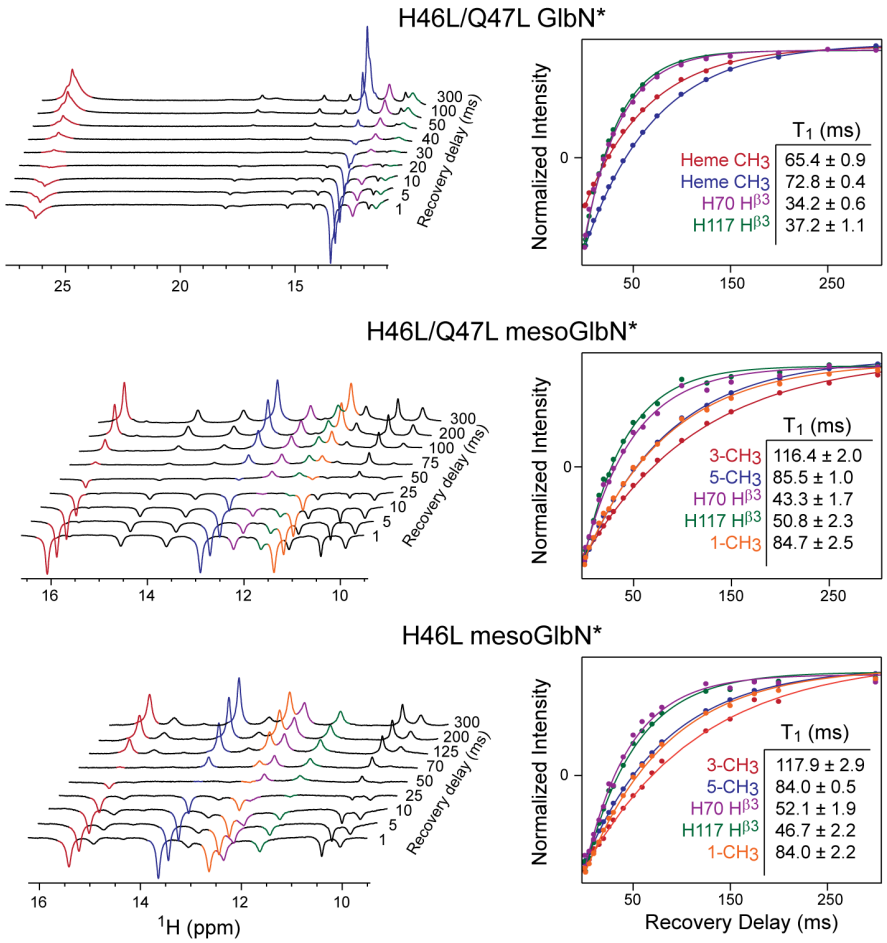

Figure S1. Inversion recovery spectra for ^{1}H T_1 determination. Data are shown for H46L/Q47L GlbN* (top, 1.7 mM GlbN, 25 mM Na/K phosphate pH* 7.5, 99% $^{2}H_2O$), H46L/Q47L mesoGlbN* (middle, 2 mM GlbN, 30 mM Na/K phosphate pH* 7.2, 99% $^{2}H_2O$) and H46L mesoGlbN* (bottom, 0.5 mM GlbN, 20 mM Na/K phosphate pH* 7.3, 99% $^{2}H_2O$). Peak heights were measured and curve fitting was used to extract T_1 values. In some cases, partial overlap rendered the fitted parameters approximate.

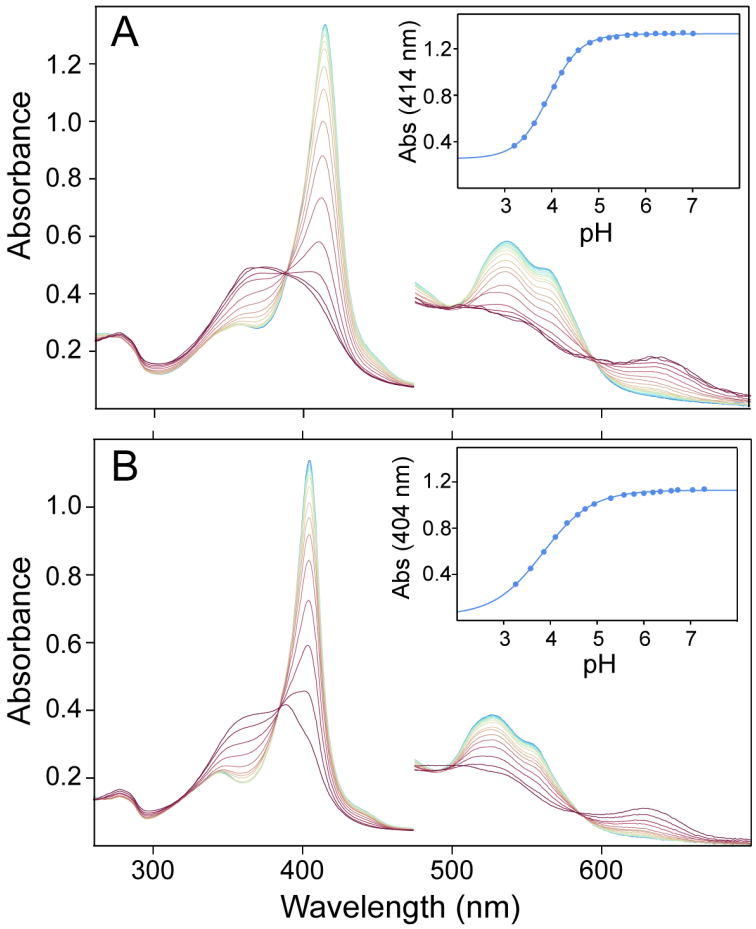

Figure S2. The pH titrations of ferric H46L/Q47L GlbN* (A, 10 μM GlbN, 5 mM Na phosphate) and ferric H46L/Q47L mesoGlbN* (B, 10 μM GlbN, 5 mM Na phosphate). The low-spin forms present at neutral pH (blue) are converted to acid denatured states (red). The broad Soret peak and charge transfer band of the acid form indicate a dissociated heme. The insets show the change in Soret absorbance as a function of pH. The solid lines represent fits to the Henderson-Hasselbalch equation. Both complexes show the same apparent pK_a for the acid transition (4.0 ± 0.1); the Hill coefficient for the mesoheme complex (B, 0.8 ± 0.1) is slightly lower than that of the *b* heme complex (A, 1.0 ± 0.1) though within fitting error. Below pH 3 additional species contribute to the optical spectra. The titration of H46L/Q47L GlbN* is practically identical to that of H46L GlbN*.[1]

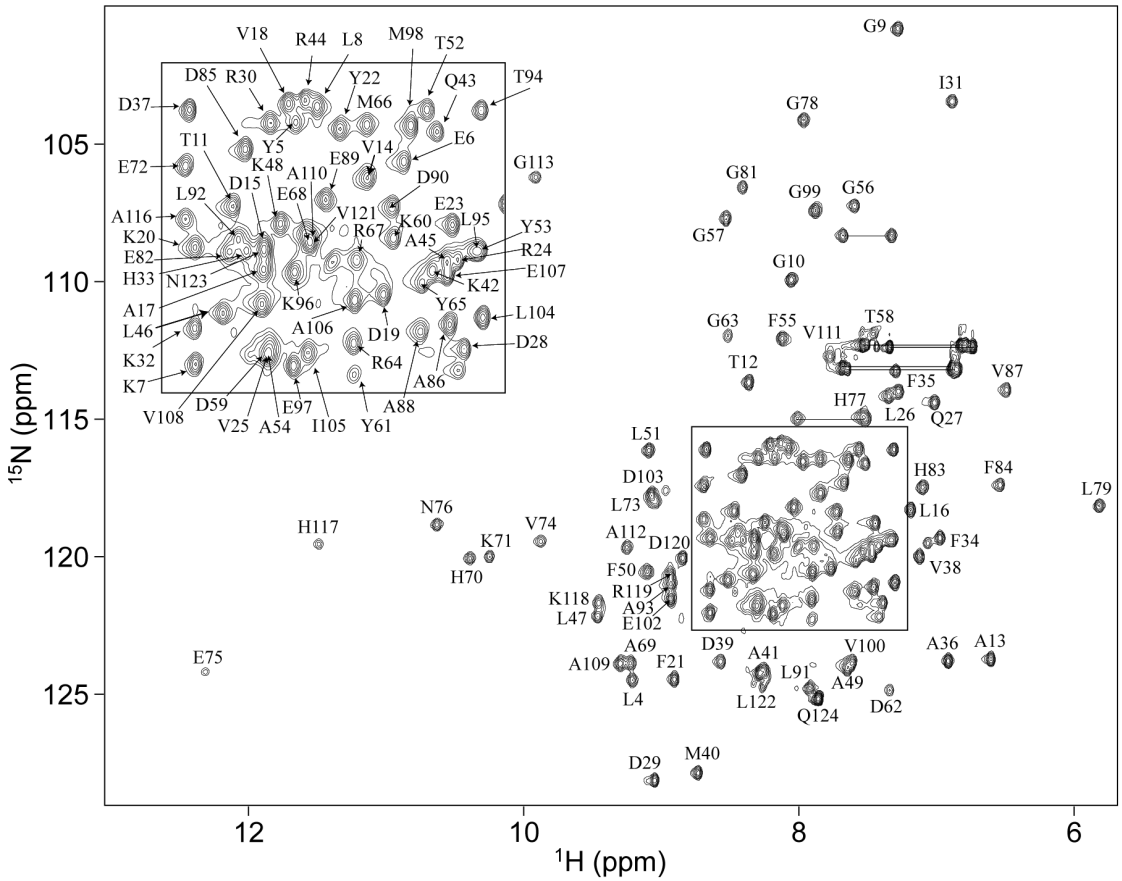

Figure S3. The annotated ^{1}H-^{15}N HSQC spectrum of H46L/Q47L mesoGlbN* (1.5 mM GlbN, 20 mM Na phosphate pH 7.1, 10% $^{2}H_2O$). The amide group Thr3 was not assigned. The signals for Asn80 and Ala114 are not visible at this contour level.

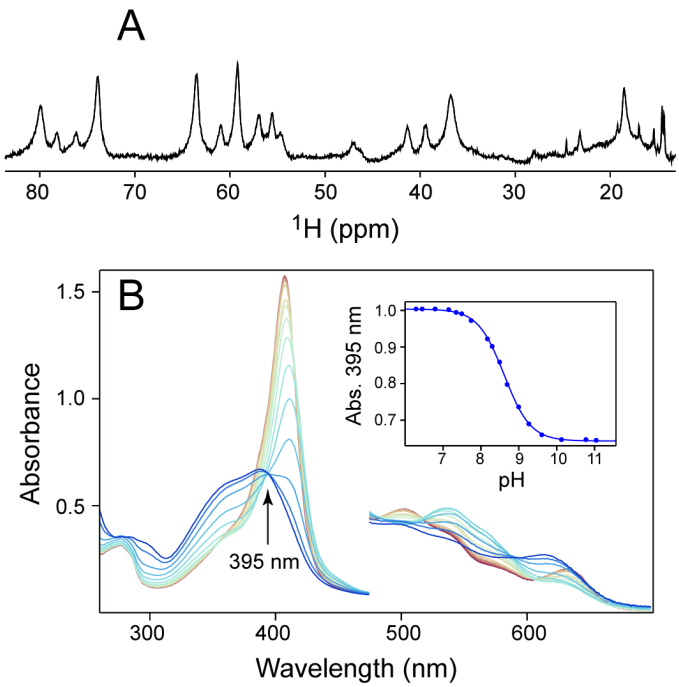

Figure S4. (A) Downfield region of the ^{1}H NMR spectrum of ferric H46L/H117A GlbN (300 μM GlbN, 20 mM Na phosphate, pH 7.1, 10% ^2H_2O). (B) The pH titration of ferric H46L/H117A GlbN (10 μM GlbN, 5 mM Na phosphate) monitored by electronic absorption spectroscopy. Spectra are colored from red (pH 6.4) to blue (pH 11.0) in a linear gradient according to pH. The inset shows the change in absorbance at 395 nm and a fit to the Henderson-Hasselbalch equation yielding a pK_a of 8.6 ± 0.1 and a Hill coefficient of 1.2 ± 0.1. Above pH ~9, base denaturation and release of the heme is observed, which interfered with accurate determination of the pK_a. The absorbance of 395 nm (apparent isosbestic point for heme loss) was chosen to assess the aquomet to hydroxymet transition.

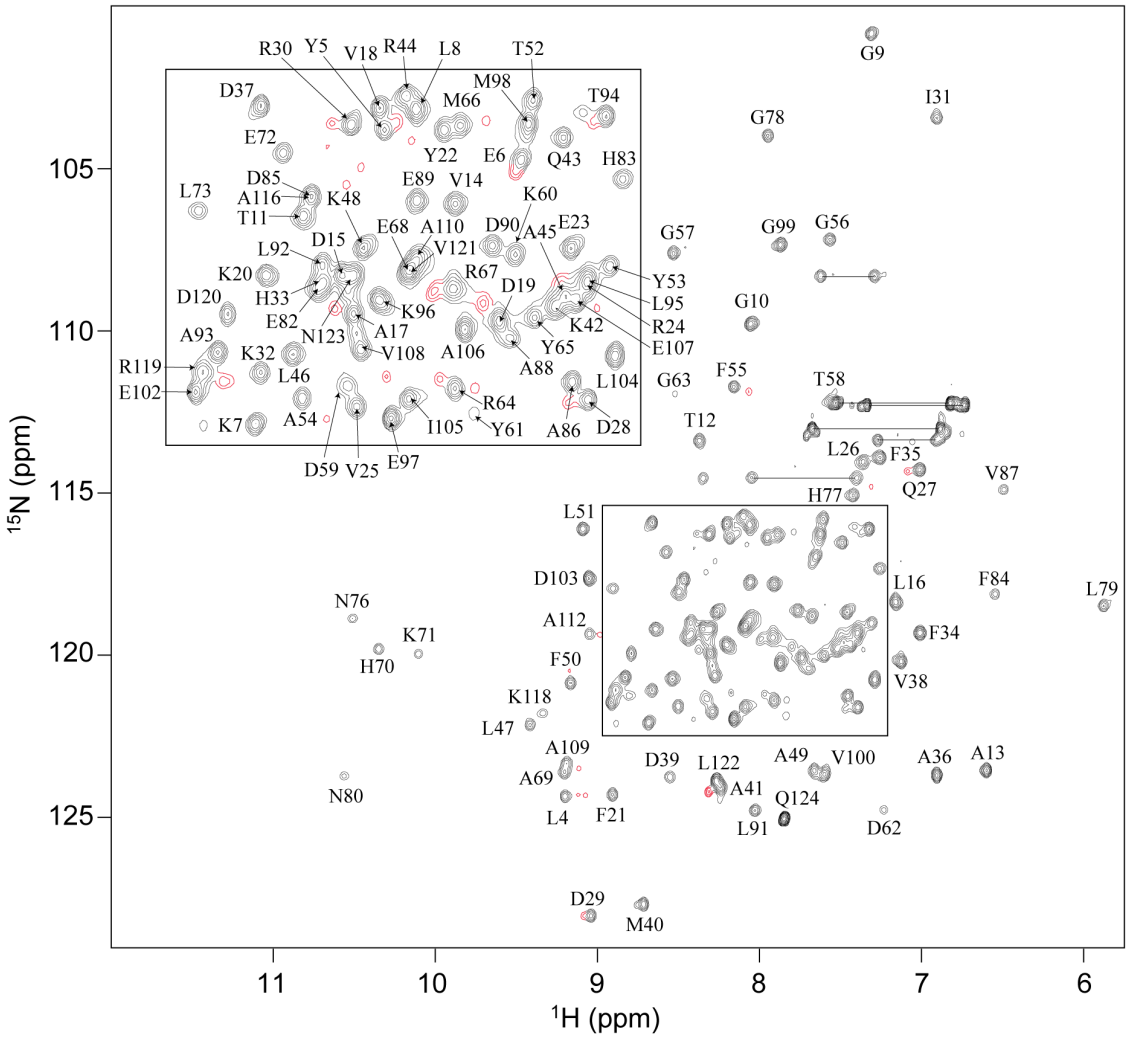

Figure S5. The annotated ^{1}H-^{15}N HSQC spectrum H46L/Q47L GlbN* (2 mM GlbN, 25 mM Na phosphate pH 7.2, 5% $^{2}H_2O$). The assignments for the major form, shown in black, are given. At this contour level, peaks arising from Val74, Glu75, Gly81, Val111, Gly113, Ala114 and His117 are not visible, while that of Thr3 could not be assigned. Correlations identified as arising from the minor form, which accounts for about 20% of the sample, are colored in red.

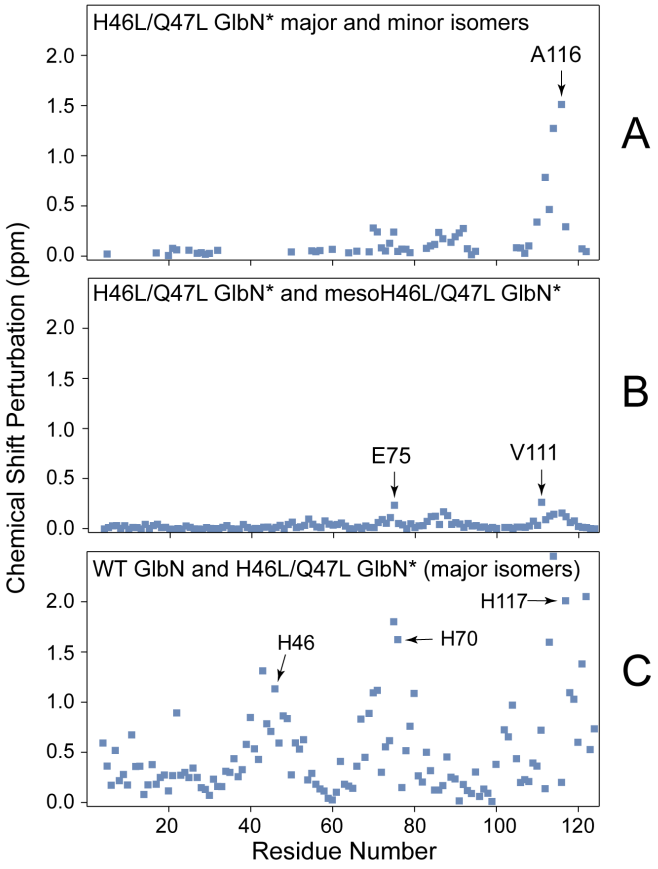

Figure S6. Comparison of ^{1}H and ^{15}N amide chemical shifts between different ferric GlbN complexes. The chemical shift perturbation is $CSP = \frac{1}{2}\sqrt{(^{H}\delta_A - ^{H}\delta_B)^2 + 0.1(^{N}\delta_A - ^{N}\delta_B)^2}$, where $^{H}\delta_A$ and $^{N}\delta_A$ represents the ^{1}H and ^{15}N amide chemical shift of species A and $^{H}\delta_B$ and $^{N}\delta_B$ those of species B. (A) The CSP between the major and minor heme rotational isomers of H46L/Q47L GlbN* (pH 7.2, 25 °C), for the subset of amides (53) assigned in the minor form. (B) The CSP between the major form of H46L/Q47L GlbN* (pH 7.2, 25 °C) and H46L/Q47L mesoGlbN* (pH 7.1, 25 °C). (C) The CSP between WT GlbN (BMRB 5269, pH 7.5, 25 °C) and the major form of H46L/Q47L GlbN* (pH 7.2, 25 °C). The largest CSPs in panels A and B, resulting from heme isomerization and mesoheme substitution, respectively, are localized around E75, F84 and A114. Saturation of the vinyl groups or heme isomerization is expected to reposition F84 and cause structural rearrangement toward the end of the H helix. Strong NOEs between F84 and the mesoheme 3-CH_3 (Figure S10A, Table S2) suggest high sensitivity of the shifts to porphyrin ring current and paramagnetism, whereas NOEs between F84 and A114 (Figure S10B) support a structural rearrangement (and sensitivity to paramagnetic effects). In addition, in GlbN*, the main chain/side chain hydrogen bond between Asn80 and His83 is perturbed. The extent of rearrangement, and the source of large changes in both ^{1}H and ^{15}N amide shifts of residues 112–116, is likely dependent on the nature and exact position of the heme. The peptide bond linking A114 and P115 was confirmed to have *trans* configuration in both heme isomers of H46L/Q47L GlbN. The large CSPs in panel C are related to structural and paramagnetic differences.

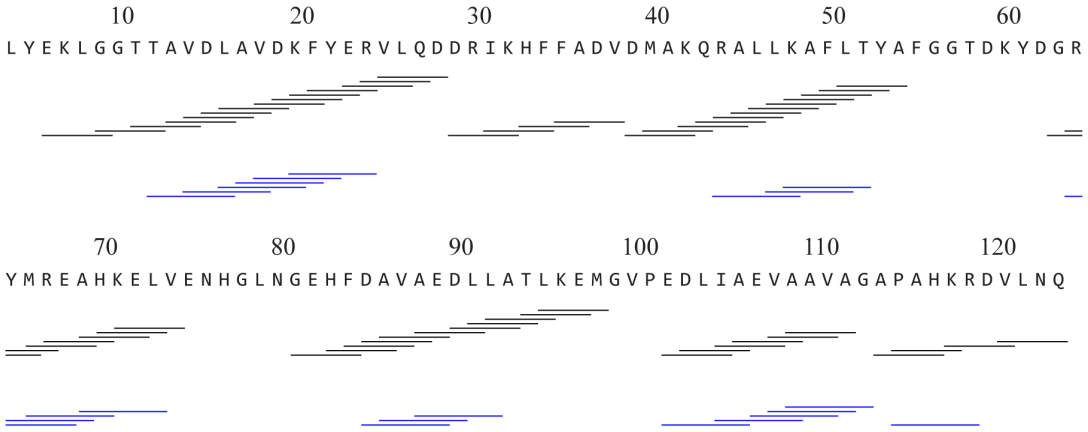

Figure S7. Medium range helical NOEs detected with a ^{1}H-^{15}N NOESY-HSQC experiment in H46L/Q47L mesoGlbN* (1.5 mM GlbN, 20 mM Na phosphate pH 7.1, 10% $^{2}H_2O$). The sequence from residues Leu4 to Gln124 is shown and the numbers are left-justified with the corresponding residue. NOEs between H^{α_i} and $H^{N_{i+3}}$ are shown in black; NOEs between H^{α_i} and $H^{N_{i+4}}$ are shown in blue. These NOEs, along with the H^{N_i}–$H^{N_{i+1}}$ and H^{N_i}–$H^{N_{i+2}}$ NOEs (not shown) correspond well to the helices predicted by TALOS+ and the helices of WT GlbN.

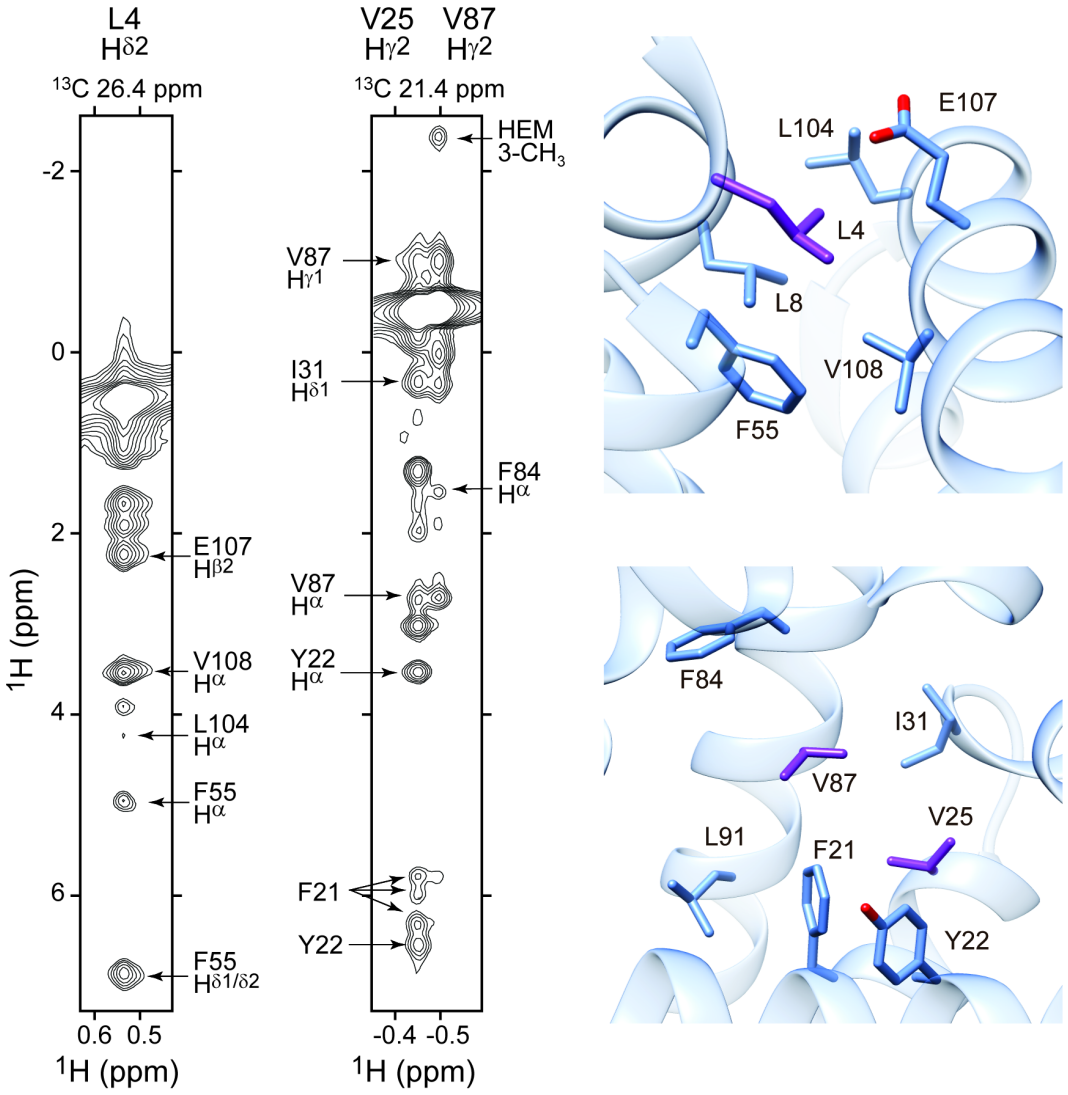

Figure S8A. Left: strips of the $^{13}CH_3$-edited NOESY spectrum of H46L/Q47L mesoGlbN* (2.5 mM GlbN, 20 mM Na phosphate, pH* 7.2, 99% ^2H_2O). Interresidue NOEs for methyl groups of L4, V25 and V87 are labeled. The mesoheme 3-CH_3 is aliased from the true ^1H shift of 16.1 ppm. Some of the annotated peaks are weak but real as can be ascertained with a lower contour level. Stereospecific assignments are arbitrarily based on the structure of the cyanomet protein. Right: portions of the cyanomet GlbN crystal structure (PDB: 1S69) showing the relevant residues. In this structure, the heme lies between F21 and F84 and is not shown for clarity.

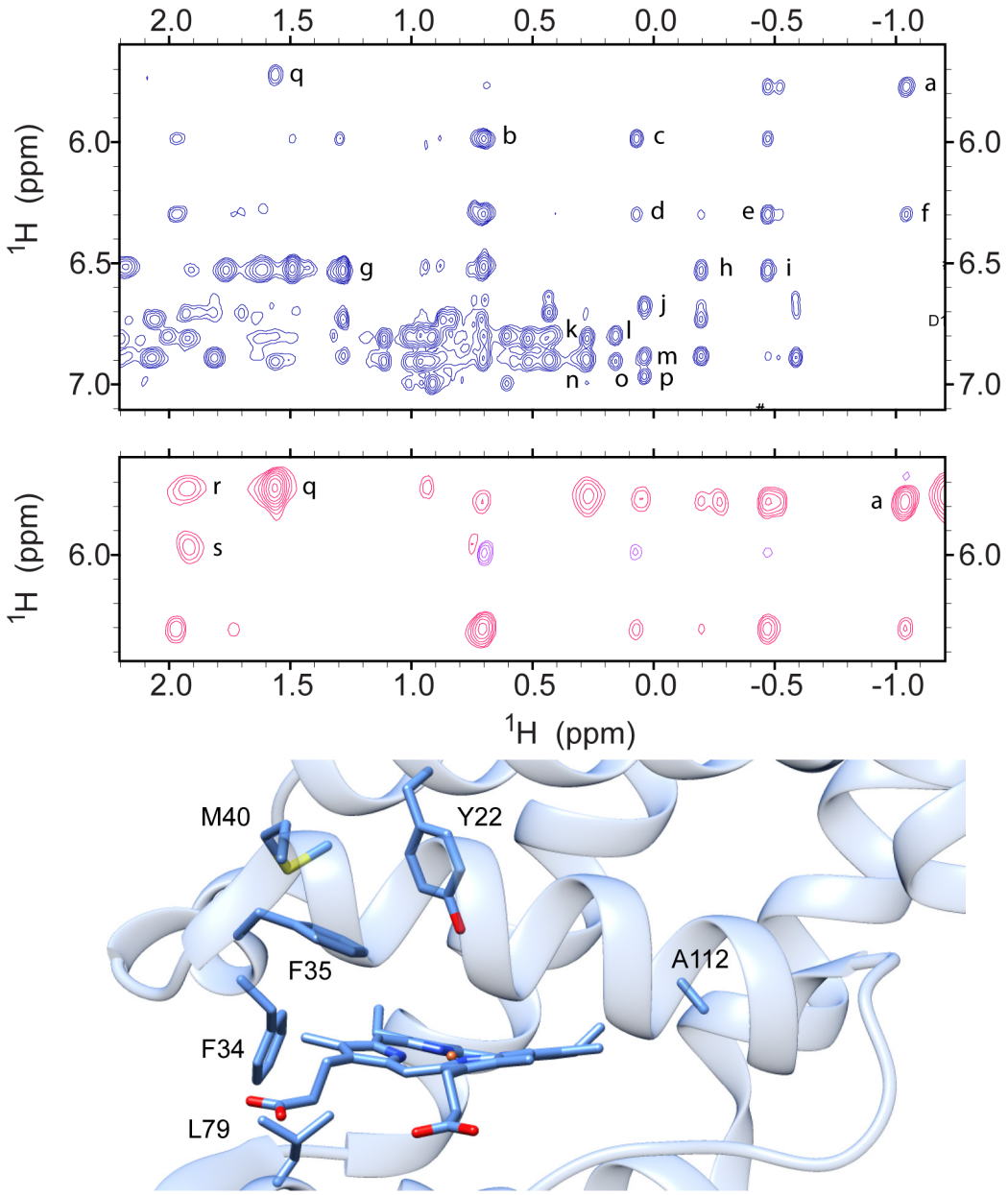

Figure S8B. Portions of the NOESY data (top, relaxation time 1.1 s, mixing time 80 ms) and WEFT-NOESY data (middle, relaxation time 30 ms, recovery time 125 ms, mixing time 40 ms) collected on H46L/Q47L mesoGlbN* (2.5 mM GlbN, 20 mM Na phosphate, pH* 7.2, 99% ^2H_2O). Some of the NOEs are labeled: F21 H^{ζ} to V87 $H^{\gamma1}$ (a); F21 $H^{\delta1/\delta2}$ to L47 $H^{\delta2}$ (b) and L91 $H^{\delta1}$ (c); F21 $H^{\varepsilon1/\varepsilon2}$ to L91 $H^{\delta1}$ (d); V25 $H^{\gamma2}$ (e) and V87 $H^{\gamma1}$ (f); Y22 $H^{\delta1/\delta2}$ to M40 H^{ε} (g), V25 $H^{\gamma1}$ (h), and V25 $H^{\gamma2}$ (i); F35 H^{ζ} to L79 $H^{\delta2}$ (j); F55 $H^{\delta1/\delta2}$ and F55 $H^{\varepsilon1/\varepsilon2}$ to L8 $H^{\delta2}$ (k); F55 $H^{\varepsilon1/\varepsilon2}$ to L51 $H^{\delta2}$ (l); F34 $H^{\delta1/\delta2}$ to L79 $H^{\delta2}$ (m); F55 H^{ζ} to L8 $H^{\delta2}$ (n) and L51 $H^{\delta2}$ (o); H77 $H^{\delta2}$ to L79 $H^{\delta2}$ (p); A112 H^{α} to A112 H^{β} (q) and 8-CH_3 (r); F50 H^{ζ} to 8-CH_3 (s). All protein methyl NOEs are confirmed in the $^{13}CH_3$-edited NOESY spectrum. The bottom panel shows some of these residues in the cyanomet GlbN structure (PDB ID 1S69). Other residues appear in Figures S8A, S9, and S10.

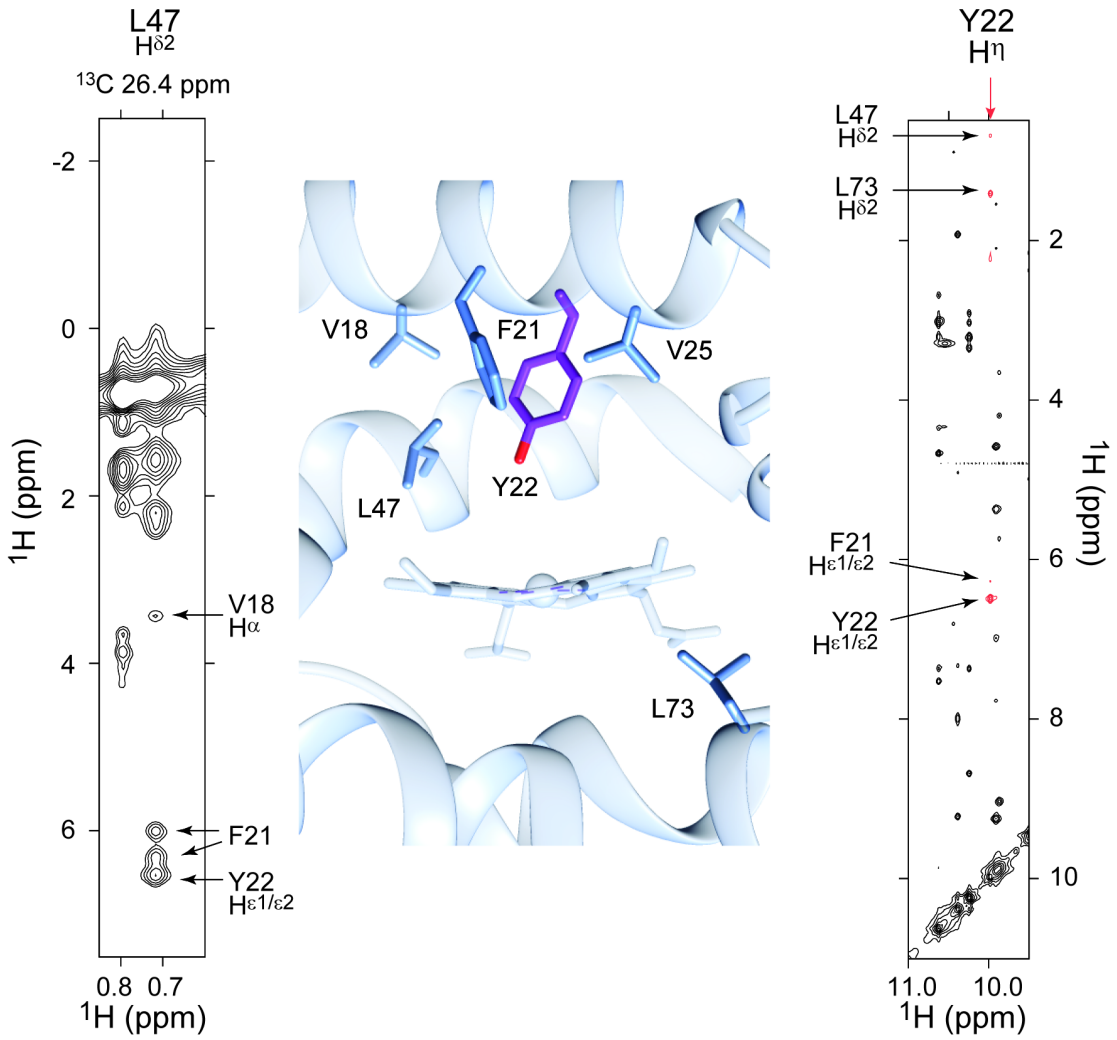

Figure S9. The environment of Tyr22 in H46L/Q47L mesoGlbN* illustrated with NOEs. A portion of the $^{13}CH_3$-edited NOESY spectrum (left, 2.5 mM GlbN, 20 mM Na phosphate, pH* 7.2, 99% ^2H_2O) shows interresidue NOEs involving L47 and V18, F21 and Y22. NOEs to Y22 H^{η} were detected with a ^1H-^1H NOESY spectrum (right, 2.0 mM GlbN, 30 mM Na phosphate, pH* 7.2, 10% ^2H_2O) and are colored in red. Contacts to F21, L47 and L73, as well as a strong intraresidue NOE are labeled. A portion of the cyanomet GlbN crystal structure (PDB: 1S69) is shown in the center (axial ligands omitted). The Q47L replacement was generated in Chimera.[2] Stereospecific assignments are arbitrarily based on the structure of the cyanomet protein. A weak NOE between L73 $H^{\delta 2}$ and Y22 $H^{\varepsilon 1/\varepsilon 2}$ is also observed in the $^{13}CH_3$-edited NOESY spectrum, but is not visible in Figure 9.

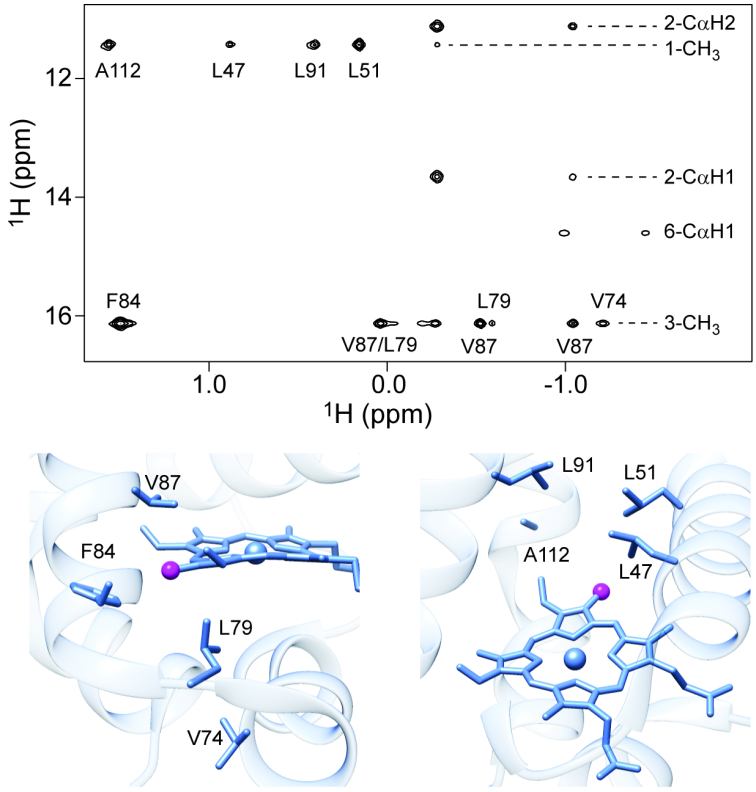

Figure S10A. Top: a portion of the ^{1}H-^{1}H NOESY acquired on H46L/Q47L mesoGlbN* (2 mM GlbN, 30 mM Na phosphate, pH* 7.2, 99% $^{2}H_2O$) shows NOEs to the mesoheme 1- and 3-CH_3. Bottom: two views of the crystal structure of cyanomet GlbN (PDB ID: 1S69, axial ligands omitted). The residues contacting the 3-CH_3 (magenta ball, bottom left) and the 1-CH_3 (magenta ball, bottom right) are labeled. The Q47L replacement was generated with Chimera.[2]

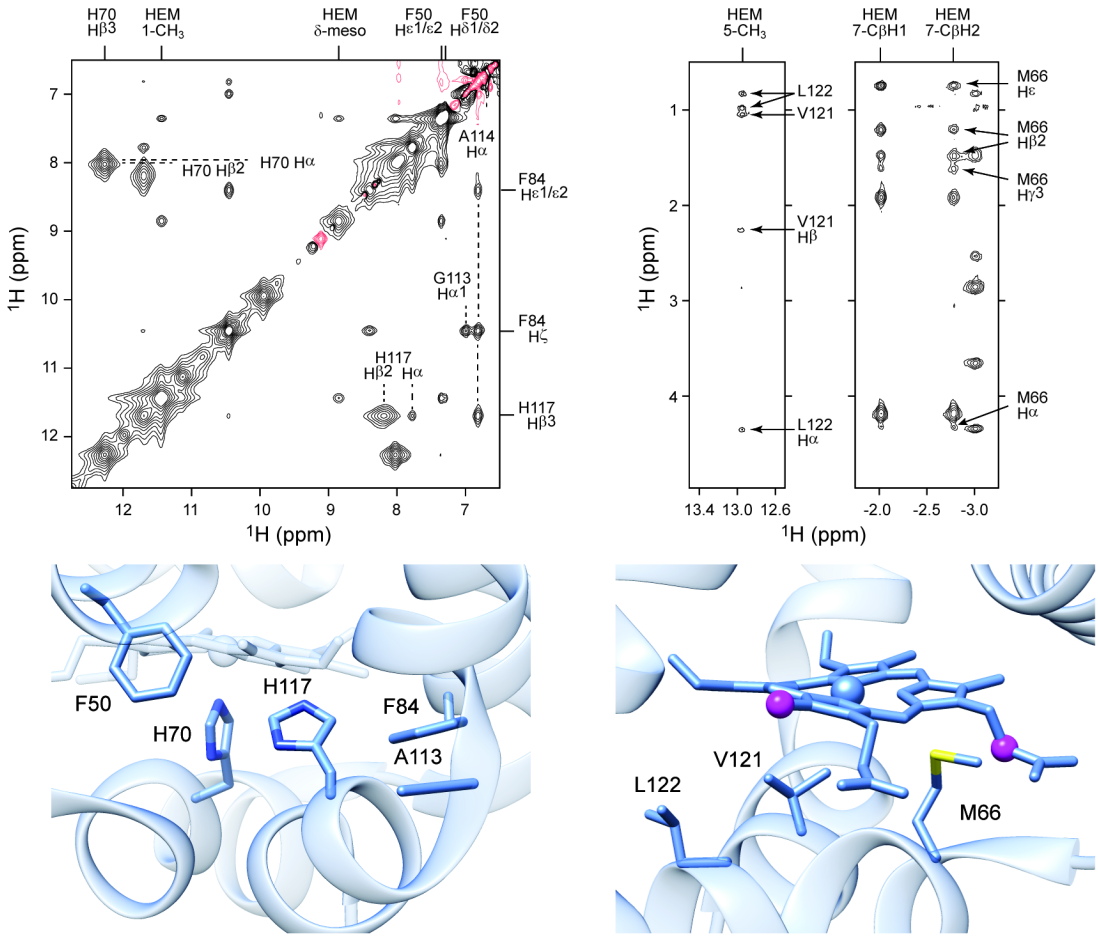

Figure S10B. Top left: NOEs among F50, H70, F84, G113, A114, H117 and mesoheme detected in ^{1}H-^{1}H WEFT-NOESY data acquired on H46L/Q47L mesoGlbN* (2 mM GlbN, 30 mM Na phosphate, pH* 7.2, 99% $^{2}H_2O$, parameters as in Figure S8B). The WEFT delays were chosen to enhance ^{1}H with short T_1 values; negative contours are colored red. Two regions of the NOESY spectrum in Figure S10A are shown at top right with a 5-fold lower contour level. NOEs between the A and D pyrroles of mesoheme and M66, V121 and L122 side chains are labeled. The crystal structure of cyanomet GlbN (PDB ID: 1S69) is shown below (axial ligands omitted). The covalent bond between *b* heme and His117 has been removed for this depiction.

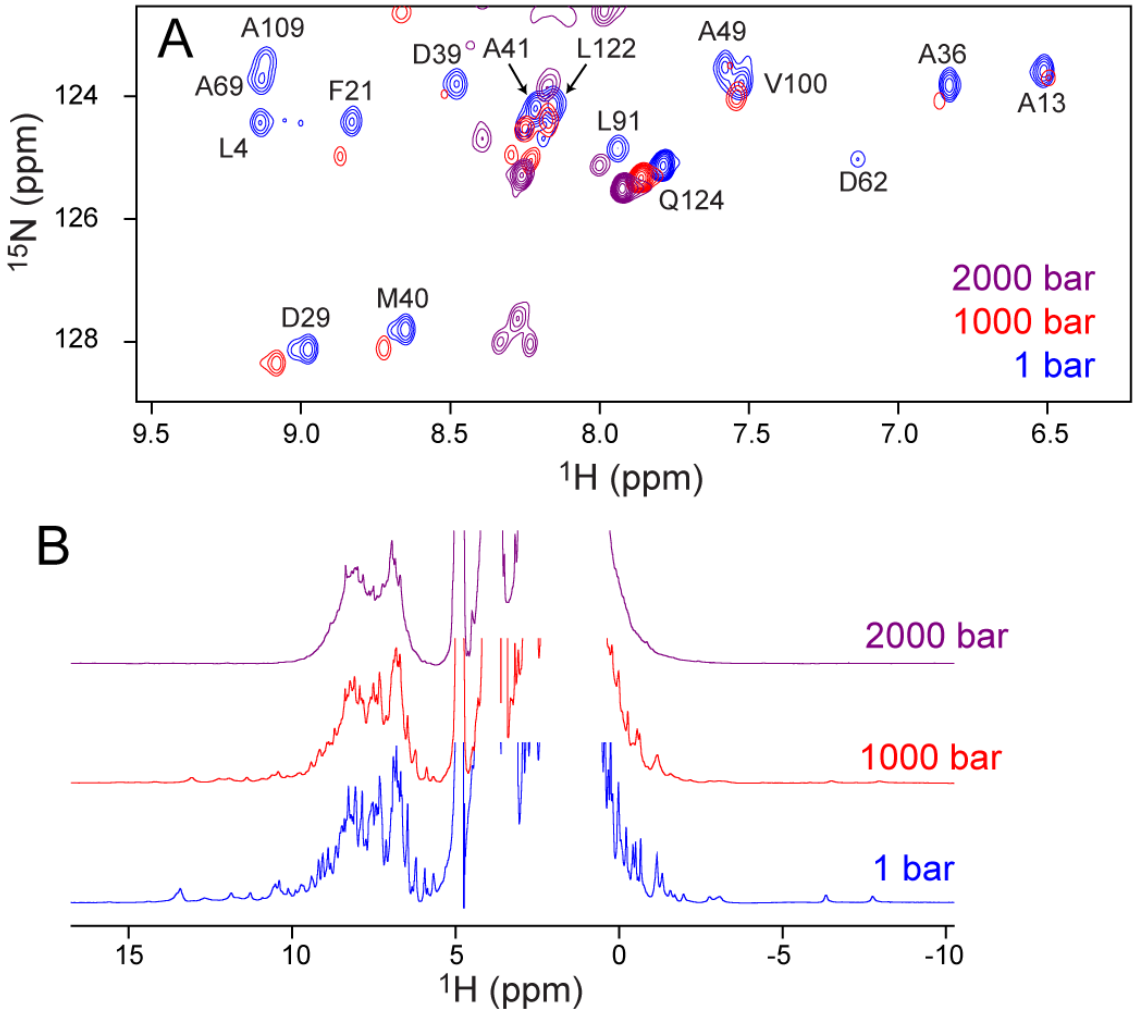

Figure S11. High pressure NMR spectra of H46L/Q46L GlbN* (0.7 mM GlbN, 14.1 mM Tris, 5.9 mM phosphate, pH 7.5 at 1 bar). The buffer was chosen to maintain constant sample pH at increasing pressures.[3] (A) ^{1}H-^{15}N HSQC spectra collected at 1 bar (blue), 1000 bar (red) and 2000 bar (purple) show denaturation of the protein. Paramagnetic effects are likely relevant to the appearance of the spectra at high pressures. Note that the behavior of Gln124 is consistent with an unstructured C-terminus at 1 bar. (B) The ^{1}H 1D spectra collected concurrently with the ^{1}H-^{15}N spectra. No hyperfine shifted peaks are apparent in the spectrum at 2000 bar.

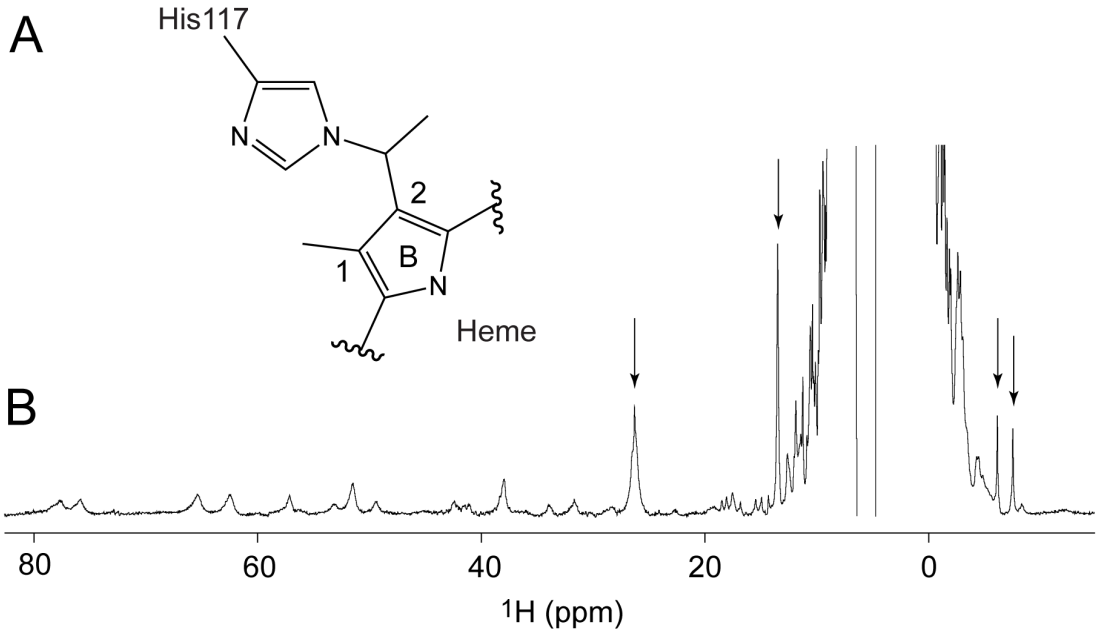

Figure S12. (A) Structure of the covalent heme–protein linkage observed in GlbN. The heme modification is formed efficiently in the WT protein by anaerobic reduction. (B) The ^{1}H NMR spectrum of a sample of H46L/Q47L GlbN* that was incubated with DT overnight, then reoxidized with ferricyanide and thoroughly buffer exchanged. Conditions are ~0.7 mM GlbN, 10% $^{2}H_2O$ 20 mM phosphate, pH 7.2. The spectrum shows the original low-spin ferric complex, denoted with black arrows, and a high-spin species with signals downfield of 40 ppm. The high-spin complex is ascribable to a portion of covalently modified H46L/Q47L GlbN.

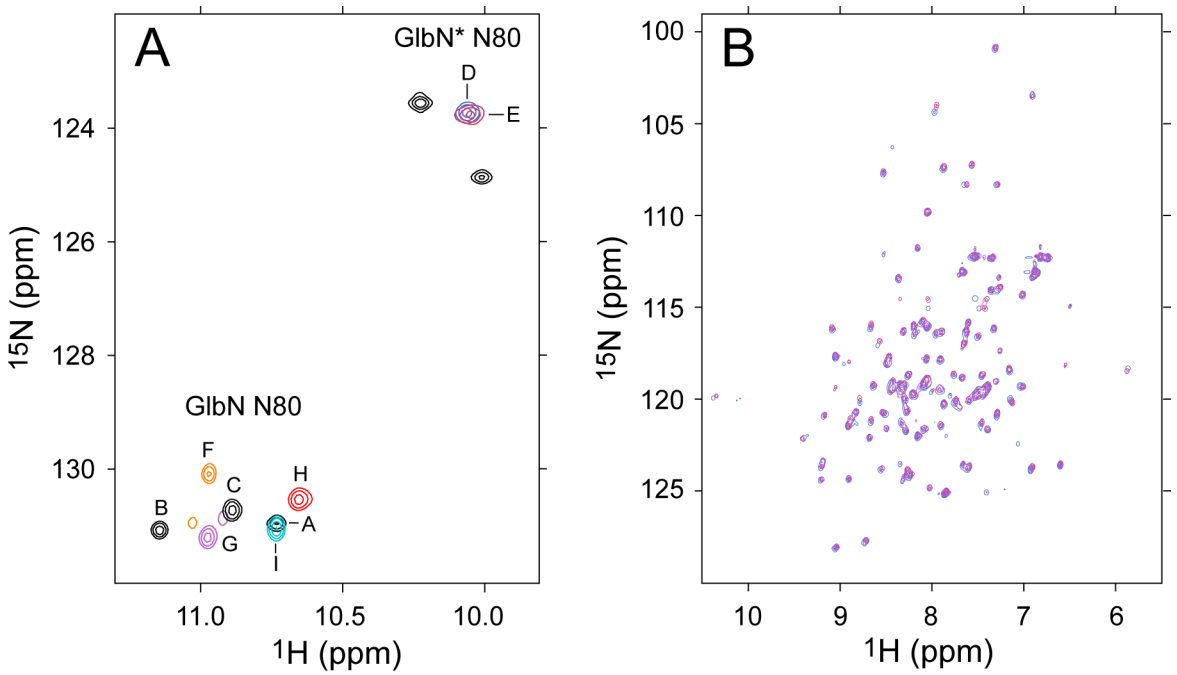

Figure S13. (A) Portions of ^{1}H-^{15}N HSQC spectra of various GlbN complexes showing the amide group of Asn80. All data collected at neutral pH and 25 °C unless otherwise noted. In ferric (A), ferrous (B, diamagnetic with His117-heme covalent linkage) and cyanomet (C, 35 °C) WT GlbN the Asn80 amide signal is downfield shifted in both ^{1}H and ^{15}N owing to a conserved helix-capping hydrogen bond to His83.[4] In ferric H46L/Q47L GlbN* (D) and mesoGlbN* (E) the upfield shift of Asn80 reflects disruption of this hydrogen bond (see Results). This signal serves as a marker for the GlbN* conformation. Upon binding cyanide to H46L/Q47L mesoGlbN* (F), or upon binding cyanide (G), imidazole (H, 100 mM imidazole pH 7.8) or azide (I, 250 mM NaN_3) to H46L/Q47L GlbN*, the downfield shift of Asn80 is restored. Exogenous ligands displace His117 and allow the heme to migrate to the canonical binding site, restoring the normal structure of the F–G turn. (B) Demonstration of the reversibility of ligand binding to GlbN*. H46L/Q47L GlbN* was converted to the imidazole-bound (100 mM imidazole) or azide-bound (250 mM NaN_3) forms. Subsequent buffer exchange completely displaced imidazole (purple spectrum) or azide (blue spectrum) to yield a complex identical to the original ferric H46L/Q47L GlbN* species (red spectrum, reproduced from Figure S5).

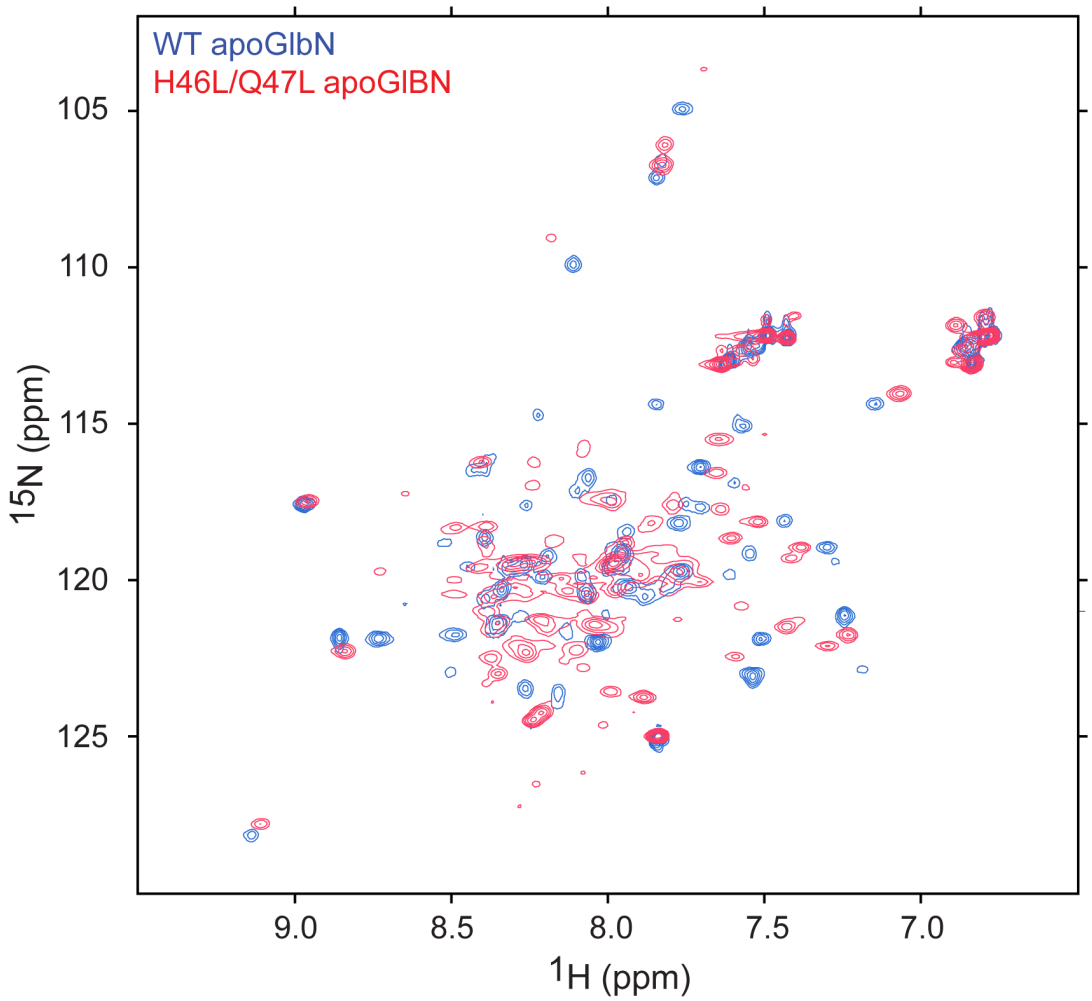

Figure S14. ^{1}H-^{15}N HSQC spectra of apoGlbNs. The spectrum of WT apoGlbN (blue, pH 7.5) displays fewer than the expected number of signals and provides evidence for conformational exchange on the chemical shift time scale. Isotopically labeled H46L/Q47L GlbN* was converted to the apoprotein (red, final conditions 0.2 mM GlbN, 0.5 mM Mb, 25 mM Na phosphate, 100 mM Tris, 2 mM EDTA, pH 7.5) by incubation for 2 h with excess unlabeled apomyoglobin. The HSQC spectrum of the variant apoGlbN (red) is broadly similar to that of the WT protein (blue). Both spectra show evidence for intermediate conformational exchange. Chemical shift differences between the WT and variant apoproteins are observed and difficult to interpret given the exchange regime. The spectra demonstrate that the apoproteins do not possess stable tertiary structure. No extensive refolding is caused by the H46L/Q47L replacements in the absence of a cofactor.

References

(1) Nothnagel, H. J., Love, N., and Lecomte, J. T. J. (2009) The role of the heme distal ligand in the post-translational modification of *Synechocystis* hemoglobin. *J. Inorg. Biochem. 103*, 107-116.

(2) Pettersen, E. F., Goddard, T. D., Huang, C. C., Couch, G. S., Greenblatt, D. M., Meng, E. C., and Ferrin, T. E. (2004) UCSF Chimera - a visualization system for exploratory research and analysis. *J. Comput. Chem. 25*, 1605-1612.

(3) Quinlan, R. J., and Reinhart, G. D. (2005) Baroresistant buffer mixtures for biochemical analyses. *Anal. Biochem. 341*, 69-76.

(4) Preimesberger, M. R., Majumdar, A., Rice, S. L., Que, L., and Lecomte, J. T. J. (2015) Helix-capping histidines: Diversity of N-H···N hydrogen bond strength revealed by $^{2h}J_{NN}$ scalar couplings. *Biochemistry 54*, 6896-6908.